Aalborg Universitet

AALBORG UNIVERSITY

DENMARK

Achieving Wireless Cable Testing of High-order MIMO Devices with a Novel Closed-form Calibration Method

Zhang, Fengchun; Fan, Wei; Wang, Zhengpeng

Publication date:
2020

Document Version
Accepted author manuscript, peer reviewed version

Link to publication from Aalborg University

Achieving Wireless Cable Testing of High-order MIMO Devices with a Novel Closed-form Calibration Method

Fengchun Zhang, Wei Fan, and Zhengpeng Wang

Abstract—Highly integrated multiple-input multiple-output (MIMO) system designs have posed great challenges to MIMO device performance testing in conventional cable conducted setups. A wireless cable method, which can achieve cable testing functionality without actual radio frequency (RF) cable connection, has recently been considered as a strong alternative to conductive testing method. However, its applicability to high-order MIMO antenna systems is mainly limited by the calibration complexity in the literature. To tackle this issue, a novel closed-form calibration method is proposed, which can largely speed up the calibration procedure and make the testing method practical for MIMO devices of arbitrary orders. Some practical factors affecting the calibration performance are discussed with numerical simulations. The proposed algorithm is further experimentally validated for a device under test (DUT) with four antennas in the 3.45-3.55 GHz frequency band. The detailed theoretical analysis together with numerical simulations and experimental validations have demonstrated the effectiveness and robustness of the proposed algorithm.

Index Terms—Wireless cable method, MIMO testing, radio channel models, over-the-air testing, millimetre wave systems

I. INTRODUCTION

Multiple-input multiple-output (MIMO) technology has found its wide applications in various wireless standards [1], [2]. Testing the performance of a MIMO device is a mandatory step and it requires that the testing solution should be fast, cost-effective and accurate. A cable conducted method, where coaxial cables are utilized to guide testing signals from the testing instrument to the device under test (DUT) antenna ports, has been dominantly employed in the industry, as illustrated in Fig. 1 (a). This method requires removing of antennas (most likely internal antennas) from the DUT to access the antenna ports. However, conducted cable testing is getting more complicated and error-prone as the antenna count increases. Furthermore, the conducted testing might be infeasible for 5G MIMO devices due to the lack of the access to the antenna ports, where antennas are expected to be integrated with the radio frequency (RF) front-end circuitry [3]. Radiated over-the-air (OTA) testing, where built-in antennas are used directly as the interface to receive/transmit test signals, will be the dominant method for future MIMO

devices, especially for millimeter wave (mmWave) enabled and high-order MIMO radio devices.

OTA testing of MIMO devices has been extensively discussed in the literature. A mode-stirred reverberation chamber (RC) method can easily emulate a rich multipath environment. However, its spatial profile is limited to statistically isotropic angular distribution [4], [5]. A multi-probe anechoic chamber (MPAC) method, though capable of reproducing realistic multi-path environments, is limited by its expensive setup cost, where extensive channel emulator (CE) resource and a large anechoic chamber might be required [6], [7]. Therefore, there is a strong need for an alternative OTA method, which can alleviate the need for large floor space and extensive radio CE resource.

A wireless (virtual) cable method, which can achieve coaxial cable testing functionality over-the-air, has been actively discussed for 5G base station (BS) demodulation testing and mmWave terminal performance testing in recent 3GPP meetings due to its capability to replace conducted cable testing [8]–[17], as illustrated in Fig. 1 (b). The main challenge of the wireless cable method is how to efficiently obtain the static coupling coefficient matrix in the calibration stage for commercial MIMO devices. In [8], the coupling coefficient matrix was directly measured with a MIMO channel sounder in a non-anechoic environment. However, this direct measurement is typically not applicable for a commercial MIMO DUT without direct access to antenna connectors. In [9], [10], the coupling coefficient matrix is calculated based on the knowledge of complex radiation patterns of the probe antennas and the DUT antennas in ideal far-field line-of-sight (LOS) propagation conditions. However, it requires a large anechoic chamber and support from a special chip-set to report DUT antenna patterns in a non-intrusive manner. In [13], it was mentioned that the coupling coefficient matrix can be estimated via channel estimation algorithms, e.g. utilizing pilot sequence. This idea might be feasible for BS type DUTs where transmitted signals can be designed and therefore known. However, it is not applicable for user equipment (UE) type DUTs, since the coupling coefficient matrix can not be reported for testing purposes. In [12], [18], a calibration method is proposed to determine the coupling coefficient matrix via tuning the complex weights at CE output ports and monitoring the average received power per DUT antenna port in the calibration stage . The method is highly attractive since the testing can be executed in a small RF shielded box to significantly reduce setup cost. Furthermore, the method works for any LTE terminal and

Fengchun Zhang, and Wei Fan are with the Antennas, Propagation and Millimeter-wave Systems section at the Department of Electronic Systems, Aalborg University, Denmark (Corresponding author: Wei Fan, wfa@es.aau.dk.)

Zhengpeng Wang is with Electronics and Information Engineering, Beihang University, Beijing, 100191, China

coming 5G terminals supporting new radio (NR) specification, without the need for special chipset support in principle, since power measurement per DUT antenna port is supported in all standard radio specifications [1], [2]. To reduce the measurement time, different ways to tune the complex weights were reported. A brute-force method (i.e. phase and amplitude exhaustive search per wireless cable connection) was reported and experimentally validated for the LTE terminal supporting 2×2 MIMO [12], [18]. However, this method is not applicable for high-order MIMO systems, due to its extremely high computational complexity. In [11], a random search method was proposed to speed up the calibration procedure. However, its complexity is still high for high order MIMO devices. Though regarded as a potential candidate for 5G demodulation testing in standardization, the wireless cable solution has not been discussed for the DUTs with more than two receive ports [14], [15].

It is desirable that the coupling coefficient matrix can be obtained accurately and reliably within a short calibration time and with a cost-effective compact measurement setup (e.g. an anechoic box). Moreover, the calibration methods should be directly applicable to any wireless devices supporting MIMO standards. At last, the complexity should not be scaled up significantly for high-order MIMO devices. However, such a method satisfying all the requirements is currently missing in the literature, to the best knowledge of the authors. In this paper, to address all the testing requirements , a novel closed-form calibration method is proposed to achieve wireless cable testing of radio devices with arbitrary MIMO orders.

The rest of this paper is structured as follows. In Section II, the principle of the closed-form calibration method is described. Section III discusses some practical factors that would affect the wireless cable connection quality with numerical simulations. The measurement results in Section IV validate the algorithm. The conclusion is provided in Section V.

II. METHOD

A. Problem Statement

As illustrated in Fig. 1 (a), for a MIMO system with M antennas at the transmitter (Tx) side and N antennas at the receiver (Rx) side, the signal model for the conducted cable setup, ignoring the noise at the Rx side and assuming balanced transmission over RF cables, can be written as:

$$\boldsymbol{y}(f,t) = \boldsymbol{s}(f,t) = \boldsymbol{H}(f,t)\boldsymbol{x}(f,t), \quad (1)$$

where we have $\boldsymbol{H}(f,t) = \{h_{n,m}(f,t)\}_{N \times M}$, with $h_{n,m}(f,t)$ the time-variant channel frequency response (CFR) from the mth Tx antenna port to the nth Rx antenna port, $\boldsymbol{y}(f,t) = \{y_n(f,t)\}_{N \times 1}$ the received signal vector at the N Rx antenna ports, $\boldsymbol{x}(f,t) = \{x_m(f,t)\}_{M \times 1}$ the transmit signal vector at the M Tx antenna ports and $\boldsymbol{s}(f,t) = \{s_n(f,t)\}_{N \times 1}$ the testing signal vector to be directed to the N Rx antenna ports. In the conducted cable setup, signals can be directed to respective antenna ports in a power balanced way, without cross talks between coaxial cables. Antenna patterns at the Tx side and the Rx side, when available, can be embedded in the CFRs implemented in the CE.
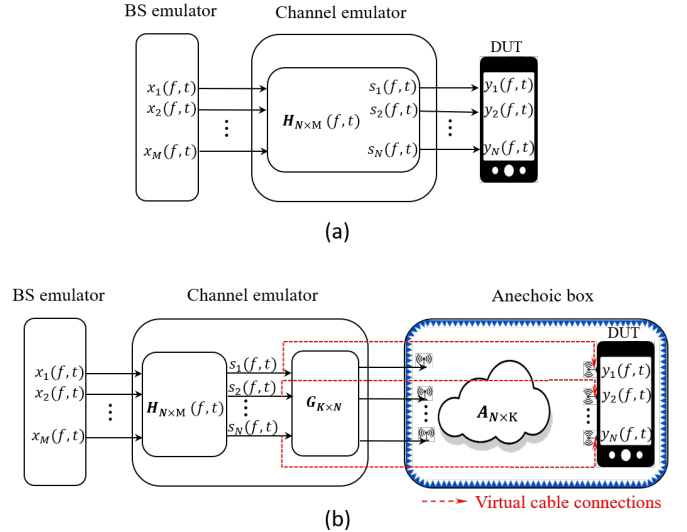

Figure 1. An illustration of the conducted cable setup (a) and the wireless cable setup (b). M, K, and N denote the number of BS antenna ports, probe antenna ports and DUT antenna ports, respectively.

As illustrated in Fig. 1 (b), the signal model for the wireless cable setup can be written as:

$$\boldsymbol{y}(f,t) = \boldsymbol{AGs}(f,t) = \boldsymbol{AGH}(f,t)\boldsymbol{x}(f,t) = \boldsymbol{H}(f,t)\boldsymbol{x}(f,t), \quad (2)$$

where $\boldsymbol{A} = \{a_{n,k}\}_{N \times K}$ is the unknown coupling coefficient matrix between the K probe antenna ports and the N DUT antenna ports. $\boldsymbol{G} \in \mathbb{C}^{K \times N}$ is the compensation matrix to achieve $\boldsymbol{AG} = \boldsymbol{I}_{N \times N}$ with $\boldsymbol{I}_{N \times N}$ denoting a $N \times N$ identity matrix. The matrix implemented in the CE for performance testing is $\boldsymbol{H}_{ce}(f,t) = \boldsymbol{GH}(f,t)$. As shown in (2), if the static coupling coefficient matrix $\boldsymbol{A}$ is known in the calibration stage, it can be calibrated out via implementing the compensation matrix $\boldsymbol{G}$ in the CE to achieve the virtual cable connection functionality.

As discussed in the introduction section, a closed-form calibration method to determine $\boldsymbol{G}$ for MIMO systems of arbitrary order in a cost-effective compact setup is still missing in the literature. Below a novel calibration method is described to address this problem.

B. Proposed Closed-form Calibration Method

The measurement setup with a wireless cable method for a $M \times N$ MIMO system is illustrated in Fig. 1 (b). Typically, each output interface of the CE is equipped with a magnitude and phase control network, as illustrated in Fig. 2. Furthermore, the average received power per DUT antenna port is typically accessible in various radio specifications. The research question can be then simplified as whether the coupling coefficient matrix $\boldsymbol{A}$ can be obtained via tuning the digital phase shifters and programmable attenuators in the CE output interface with power measurements per DUT antenna port. In the calibration stage, the emulated channel models $\boldsymbol{H}(f,t)$ are bypassed in the CE [11], [18]. As shown in Fig. 2, the composite coupling coefficient from the OTA probe ports
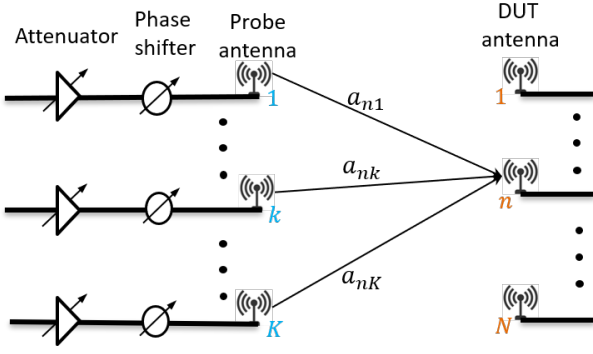
Figure 2. An illustration of the system configuration for the wireless cable method.

to the nth DUT antenna port, with phases set to 0° for all phase shifters and attenuation set to 0 dB for all attenuators in the CE, can be given by:

$$a_n^o = \sum_{k=1}^{K} a_{nk}. \qquad (3)$$

The complex composite coefficient can be given as $a_n^o = \alpha_n^o e^{j\varphi_n^o}$ with α_n^o and φ_n^o denoting its amplitude term and phase term, respectively. Let us denote the coupling coefficient from the kth probe antenna port to the nth DUT antenna port as $a_{nk} = \alpha_{nk} e^{j\varphi_{nk}}$, with α_{nk} and φ_{nk} representing the amplitude and phase terms, respectively. Our target is to estimate a_{nk} for $n \in [1, N]$ and $k \in [1, K]$. In this paper, the amplitude term α_{nk} and the phase term φ_{nk} are estimated separately, as detailed below.

1) Amplitude term estimation: The amplitude term α_{nk} can be obtained via a simple on-off operation of each probe antenna. Therefore, the kth probe antenna is enabled (via setting attenuation 0 dB in the corresponding programmable attenuator) and all other $K - 1$ probe antennas are disabled. The power recorded per DUT antenna port is monitored to obtain the amplitude term $\{\alpha_{nk}\}$ with $n \in [1, N]$ for the kth probe antenna directly from the power measurements.

2) Phase term estimation: In order to estimate phase term $\{\varphi_{nk}\}$, the attenuators connected to the probe antennas are set to 0 dB, and only the phase shifter of the kth probe is tuned with all the others fixed to zero-degree phase states. When the phase shifter of the kth probe is set to ϕ_q, the composite coupling coefficient from the OTA probe ports to the nth DUT antenna port becomes:

$$a_n^{kq} = (a_n^o - a_{nk}) + a_{nk} e^{j\phi_q} = a_{n\bar{k}} + a_{nk} e^{j\phi_q}, \qquad (4)$$

where $a_{n\bar{k}}$ denotes the composite coupling coefficient from the $(K-1)$ probe antenna ports (except the kth probe antenna port) to the nth DUT antenna port.

By setting the phase states $\{\phi_1, ...\phi_q, ...\phi_Q\}$ to the kth probe antenna and the phase state 0° to the other probe antennas, the power received by the nth DUT antenna, denoted as $\{p_n^{k1}, ...p_n^{kq}, ...p_n^{kQ}\}$, respectively, can be calculated by the composite coupling coefficient. According to (4), it yields:

$$\begin{aligned} p_n^{kq} &= (a_{n\bar{k}} + a_{nk} e^{j\phi_q})(a_{n\bar{k}} + a_{nk} e^{j\phi_q})^* \\ &= \underbrace{(\alpha_{n\bar{k}}^2 + \alpha_{nk}^2)}_{x_1} + \underbrace{\alpha_{n\bar{k}}\alpha_{nk} e^{j(\varphi_{n\bar{k}} - \varphi_{nk})}}_{x_2} e^{-j\phi_q} \\ &\quad + \underbrace{\alpha_{n\bar{k}}\alpha_{nk} e^{-j(\varphi_{n\bar{k}} - \varphi_{nk})}}_{x_3} e^{j\phi_q}. \end{aligned} \qquad (5)$$

This equation can be re-written in a matrix form as:

$$\begin{bmatrix} 1 & e^{-j\phi_1} & e^{j\phi_1} \\ \vdots & \vdots & \vdots \\ 1 & e^{-j\phi_q} & e^{j\phi_q} \\ \vdots & \vdots & \vdots \\ 1 & e^{-j\phi_Q} & e^{j\phi_Q} \end{bmatrix} \begin{bmatrix} x_1 \\ x_2 \\ x_3 \end{bmatrix} = \begin{bmatrix} p_n^{k1} \\ \vdots \\ p_n^{kq} \\ \vdots \\ p_n^{kQ} \end{bmatrix} \qquad (6)$$

$$\boldsymbol{W}\boldsymbol{x} = \boldsymbol{p},$$

where the unknowns x_1, x_2 and x_3 can be obtained via solving the linear equations in (6). According to (5), the term $\alpha_{n\bar{k}} = \sqrt{x_1 - \alpha_{nk}^2}$ is calculated with α_{nk} estimated in the previous step, and $(\varphi_{n\bar{k}} - \varphi_{nk}) = \angle x_2$ with $\angle()$ denoting the phase term of a complex value.

The ratio γ of a_{nk} to a_n^o is derived as:

$$\begin{aligned} \gamma &= \frac{a_{nk}}{a_n^o} \\ &= \frac{a_{nk}}{a_{n\bar{k}} + a_{nk}} \\ &= \frac{\alpha_{nk} e^{j\varphi_{nk}}}{\alpha_{n\bar{k}} e^{j\varphi_{n\bar{k}}} + \alpha_{nk} e^{j\varphi_{nk}}} \\ &= \frac{\alpha_{nk}}{\alpha_{n\bar{k}} e^{j(\varphi_{n\bar{k}} - \varphi_{nk})} + \alpha_{nk}}. \end{aligned} \qquad (7)$$

The ratio γ can be obtained, since α_{nk}, $\alpha_{n\bar{k}}$ and $(\varphi_{n\bar{k}} - \varphi_{nk})$ are all estimated. According to (7), the phase term of γ is expressed as:

$$\angle\gamma = \varphi_{nk} - \varphi_n^o, \qquad (8)$$

where φ_n^o is the phase term of a_n^o in (3). This phase term φ_n^o is unknown, fixed and irrelevant to probe antenna index k. The phase term of γ is taken as the estimated phase term $\hat{\varphi}_{nk}$ as:

$$\hat{\varphi}_{nk} = \varphi_{nk} - \varphi_n^o. \qquad (9)$$

The phase estimate $\hat{\varphi}_{nk}$ for $k \in [1, K]$ has a common phase offset φ_n^o.

With the estimated α_{nk} and $\hat{\varphi}_{nk}$, the estimated complex coupling coefficient is found as:

$$\hat{a}_{nk} = \alpha_{nk} e^{j\hat{\varphi}_{nk}}. \qquad (10)$$

The estimated coupling coefficient matrix $\hat{\boldsymbol{A}}$ can be therefore written as:

$$\hat{\boldsymbol{A}} = \begin{bmatrix} e^{-j\varphi_1^o} & & \\ & \ddots & \\ & & e^{-j\varphi_N^o} \end{bmatrix}_{N \times N} \boldsymbol{A}_{N \times K}. \qquad (11)$$

By implementing $\boldsymbol{G} = \hat{\boldsymbol{A}}^{-1}$, the $\boldsymbol{AG}$ term in (2) can be given as:

$$
\begin{aligned}
|\boldsymbol{AG}| &= |\boldsymbol{A}\hat{\boldsymbol{A}}^{-1}| \\
&= \left| \boldsymbol{A}\boldsymbol{A}^{-1} \begin{bmatrix} e^{j\varphi_1^o} & & \\ & \ddots & \\ & & e^{j\varphi_N^o} \end{bmatrix} \right| \\
&= \left| \begin{bmatrix} e^{j\varphi_1^o} & & \\ & \ddots & \\ & & e^{j\varphi_N^o} \end{bmatrix} \right| \\
&= \boldsymbol{I}_{N \times N}.
\end{aligned}
\tag{12}
$$

Therefore, the estimated coupling coefficient matrix $\hat{\boldsymbol{A}}$ can be used to calibrate out the coupling coefficient matrix $\boldsymbol{A}$ and the wireless cable connections can be effectively established. As with the cable conducted setup, the wireless cable method offers no cross-talks between virtual cables and a balanced power loss per virtual cable in the ideal case. Note that the relative phase difference among virtual cables will not affect the throughput measurements, same as in the conducted cable setup.

After the calibration procedure, wireless (virtual) cable connections (i.e. no cross-talk between the direct link and cross-talk links, and power balanced direct links) are established, via setting $\boldsymbol{H}_{ce}(f,t) = \boldsymbol{GH}(f,t) = \hat{\boldsymbol{A}}^{-1}\boldsymbol{H}(f,t)$ in the CE. Actual throughput measurements can be performed under desired propagation channel models $\boldsymbol{H}(f,t)$. The wireless cable setup is attractive, since the DUT can stay untouched during the whole measurement, which implies that the testing can be done in a fully automated manner. The calibration procedure and the actual performance testing with specified channel models can be performed smoothly, without operator intervention. As explained, a closed-form calibration method is proposed, which can achieve the wireless cable connections for a DUT with N antenna ports via conducting only $3K + 1$ power measurements (i.e. K on-off operations for amplitude term estimation and $2K + 1$ phase tuning operations for phase term estimation). Furthermore, an unique advantage of the proposed wireless cable method, compared to the state-of-art MPAC and radiated two stage (RTS) methods, is that the DUT can be placed in the near-field of the probe antennas. Therefore, the testing can be done in a small and movable anechoic shielded box. For a non-automated measurement system discussed in [18], it took around three minutes to perform 200 power measurements in the calibration stage. Therefore, the calibration procedure can be done within seconds for most MIMO devices with the proposed closed-form calibration method.

III. Wireless cable connection quality evaluation

In practice, (12) can only be approximated due to the unavoidable amplitude and phase uncertainties in phase shifters, and noise present in the DUT receiver, etc. The performance of the wireless cable method is evaluated by isolation levels of established wireless connections [11]. A high isolation level represents a good wireless cable performance. Below, we discuss how the phase setting matrix $\boldsymbol{W}$, the coupling coefficient matrix $\boldsymbol{A}$ and signal to noise ratio (SNR) at the receiver would affect the wireless cable performance in numerical simulations.

A. Phase setting matrix $\boldsymbol{W}$

To solve the three unknowns x_1, x_2 and x_3 in (6), $Q \geq 3$ is required. The condition number of a matrix $\boldsymbol{W}$ is defined as:

$$
\kappa(\boldsymbol{W}) = \|\boldsymbol{W}\| \cdot \|\boldsymbol{W}^+\|,
\tag{13}
$$

where $\|\cdot\|$ denotes the Euclidean norm of the matrix and $\boldsymbol{W}^+$ indicates the pseudo inverse of the matrix $\boldsymbol{W}$. Note that the condition number always satisfies $\kappa(\boldsymbol{W}) \geq 1$. The relative error in $\boldsymbol{x}$ in (6), according to the matrix theory [28], follows that

$$
\frac{\|\hat{\boldsymbol{x}} - \boldsymbol{x}\|}{\|\boldsymbol{x}\|} \leq \kappa(\boldsymbol{W})(\rho_{\boldsymbol{W}} + \rho_{\boldsymbol{p}}),
\tag{14}
$$

where $\rho_{\boldsymbol{W}}$ and $\rho_{\boldsymbol{p}}$ represent the relative error in $\boldsymbol{W}$ and $\boldsymbol{p}$, respectively. That is, the relative error in $\boldsymbol{x}$ is bounded by $\kappa(\boldsymbol{W})(\rho_{\boldsymbol{W}} + \rho_{\boldsymbol{p}})$. The matrices with small condition numbers are desirable, since they do not magnify errors, either those due to noise in the measured data, or those introduced by quantization errors of phase shifters. Phase shifters with bit-number no less than 2 are required to ensure $Q \geq 3$. According to (6), Q phase states should be set for each OTA probe and QK power measurements are required (if $\phi_1 \neq 0^o$) in the phase term estimation step. In practice, via setting $\phi_1 = 0^o$ for all OTA probes in phase estimation step, the number of power measurements is reduced to $(Q-1)K + 1$, since only $(Q-1)K + 1$ unique phase states are set in phase shifters. For practical phase shifters, the phase states are limited, depending on the phase shifter bit-number. For example, a condition number of 2 can be achieved with a 2-bit phase shifter (i.e. with $\phi_1 = 0^o, \phi_2 = 90^o$ and $\phi_3 = 180^o$). For a 4-bit phase shifter (i.e. with a least significant bit (LSB) 22.5^o), the achieved condition number is illustrated in Fig. 3, where a minimum condition number of around 1.2 can be achieved.

Intuitively speaking, increasing the number of measurements (i.e. phase states) can improve the accuracy. This is due to the fact the measurement uncertainties can be averaged out from the statistical point of view. However, this might not be the case in our analysis. The reason is that the condition numbers for different phase setting matrices $\boldsymbol{W}$ are different. Therefore, by introducing more measurements with bad-conditioned phase setting matrices $\boldsymbol{W}$, the measurement accuracy might deteriorate.

B. Coupling coefficient matrix $\boldsymbol{A}$

In the wireless cable method, the power values in (6) are recorded per carrier over the system bandwidth (e.g. up to 20 MHz for LTE system), assuming frequency flat channel. Therefore, the proposed wireless cable method only works when the coupling coefficient matrix $\boldsymbol{A}$ is frequency flat over the considered bandwidth. However, if the RF enclosure is highly reflective, for instance, a reverberation chamber, the
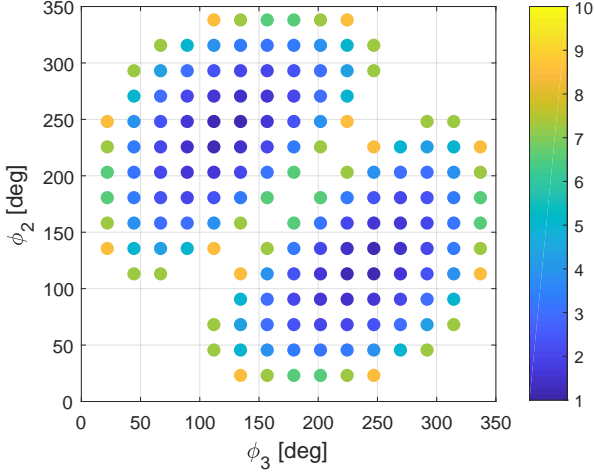
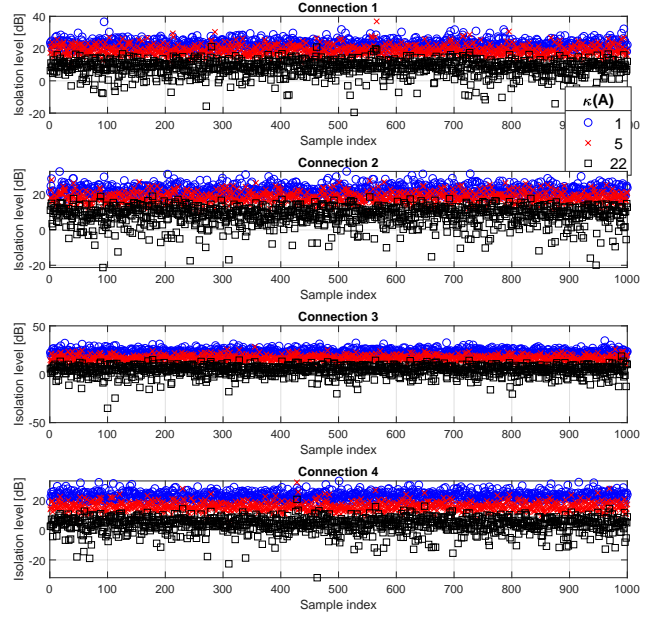Figure 3. Achieved condition number with 4-bit phase shifters. $\phi_1 = 0^o$ is set in the simulation.

Figure 4. Achieved isolation levels for matrices $\boldsymbol{A}$ with various condition numbers.

Figure 5. Statistics of the achieved isolation levels for matrices $\boldsymbol{A}$ with various condition numbers.

channels become frequency selective. As demonstrated in [19], the wireless cable method would not work in highly reflective environment. Below, we discuss how the coupling coefficient matrix $\boldsymbol{A}$ affects the wireless cable quality, assuming the matrix $\boldsymbol{A}$ is frequency flat over the bandwidth of interest.

The condition number of the matrix $\boldsymbol{A}$, i.e., $\kappa(\boldsymbol{A})$, can significantly affect the wireless cable performance. In order to demonstrate it, 4×4 matrices $\boldsymbol{A}$ with various condition numbers are synthesized. In numerical simulations, $\hat{a}_{nk}$ in (10) is given by

$$\hat{a}_{nk} = a_{nk}\epsilon, \tag{15}$$

where ϵ denotes a random complex value with amplitude and phase terms uniformly distributed within $[-1, 1]$ dB and $[-10^o, 10^o]$, respectively. The isolation levels of the wireless cables are then computed based on $|\boldsymbol{A}\hat{\boldsymbol{A}}^{-1}|$. For each matrix $\boldsymbol{A}$, 1000 $\hat{\boldsymbol{A}}^{-1}$ are generated according to (15). The achieved isolation levels of matrices $\boldsymbol{A}$ with various condition numbers are plotted in Fig. 4. As expected, a matrix $\boldsymbol{A}$ with a smaller condition number is less likely to be affected by the noise than the one with a larger condition number. The mean and standard deviations of the isolation levels are further calculated and the statistical results for matrices $\boldsymbol{A}$ with different condition numbers are ploted in Fig. 5. It shows that the achieved isolation levels of all wireless cables decrease as the condition number of the matrix $\boldsymbol{A}$ increases.

The amplitude dynamic range of a matrix $\boldsymbol{A}$ is defined as:

$$\mu(\boldsymbol{A}) = \frac{\max\limits_{n,k}\left\{|a_{nk}|\right\}}{\min\limits_{n,k}\left\{|a_{nk}|\right\}}. \tag{16}$$

The investigation of whether $\mu(\boldsymbol{A})$ will affect the condition number of the $\boldsymbol{A}$ matrix is done, via analyzing with synthetic data. 4×4 $\boldsymbol{A}$ matrices are randomly generated with a given amplitude dynamic range and random phases. The condition number distribution of all samples are analyzed by calculating the percentage of matrices $\boldsymbol{A}$, defined as:

$$\eta(\kappa_o) = \frac{\text{count}(\kappa(\boldsymbol{A}) \leq \kappa_o)}{L}, \tag{17}$$

where $\text{count}(\cdot)$ gives the number of samples satisfying a given condition and L denotes the total number of samples. In Fig. 6, $\eta(\kappa_o)$ for $\boldsymbol{A}$ matrices with different amplitude dynamic ranges $\mu(\boldsymbol{A})$ are compared. The figure shows that the condition number distributions for matrices $\boldsymbol{A}$ with various amplitude dynamic ranges are quite similar among four curves with different amplitude dynamic ranges. The results demonstrate that the condition number of a matrix $\boldsymbol{A}$ is not sensitive to the amplitude dynamic range of this matrix. As a result, the
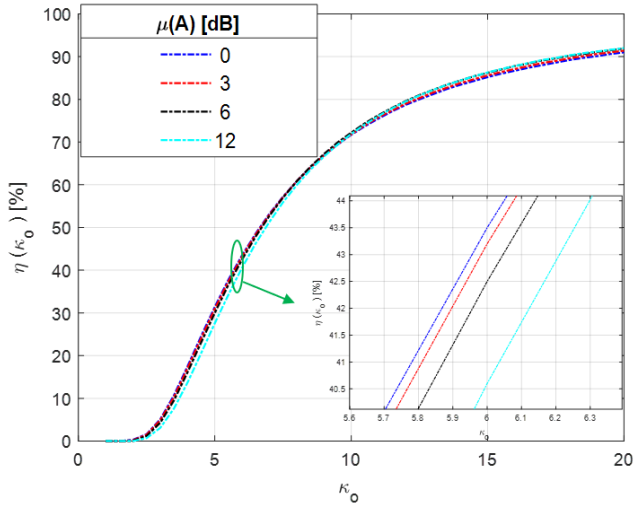
Figure 6. A comparison of the percentages of the condition numbers for matrices $\boldsymbol{A}$ with various amplitude dynamic ranges.

wireless cable performance is not determined by the amplitude dynamic range of the coupling coefficient matrix $\boldsymbol{A}$.

C. SNR

The SNR at each DUT antenna port is an important factor that affects the performance of the wireless cable method. The relative error of $\boldsymbol{x}$ in (6) is bounded by $\kappa(\boldsymbol{W})(\rho_{\boldsymbol{W}} + \rho_{\boldsymbol{p}})$. The SNR at each DUT antenna port determines $\rho_{\boldsymbol{p}}$ (the relative error in $\boldsymbol{p}$). The higher the SNR at each DUT antenna port is, the smaller the relative error in $\boldsymbol{p}$ and the more accurate estimates of $\boldsymbol{x}$ can be achieved, leading to better calibration performance. However, it is not a problem in a practical setup. Noise is typically internally generated at the Rx. In the calibration stage, the signal level is set much higher than the internal noise of the Rx. Once the calibration process is done, a good wireless cable connection is established. In the hardware emulation, although the noise is internally generated in the Rx in any cases, its exact level, however, is typically not known. Therefore, the noise needs to be emulated, which dominates over the internal "self noise", to achieve the intended SNR in the Rx. The SNR can be controlled in the hardware emulation such that the signal level is rather high and the noise power is adjusted accordingly. Note that the SNR control will not affect the wireless cable connection quality, since it is done under high signal level and no hardware emulated noise (only internal noise on the Rx, which is very small). Both the signal and hardware generated noise will be guided to the respective antenna ports, via the achieved wireless cable connections. Furthermore, it has been demonstrated in the MIMO OTA harmonization campaign that same throughput results can be achieved with the MPAC and the radiated two stage method under various SNR conditions for 2×2 MIMO systems [20]. This is also an indication that the wireless cable method works for various SNR conditions, once good wireless cable connection quality is established in the calibration stage.

IV. MEASUREMENT VALIDATION

Active throughput measurements of high-order MIMO devices under spatial fading channel conditions are not available due to lack of experimental facilities for the moment. As an alternative, a measurement system is designed without the CE and commercial high-order MIMO devices to validate the proposed calibration procedure in the laboratory.

A. Measurement Setup

An illustration of the measurement system is shown in Fig. 7, where it consists of:

- a two-port vector network analyzer (VNA).
- a magnitude and phase control network which includes a power splitting circuit, a digital phase shifter and programmable attenuator matrix connected to the probe antennas.
- 4 wideband dual-polarized quad ridged horn antennas as probe antennas. Each probe antenna has an aperture of 72 mm $\times$ 72 mm and a gain of 8.2 dBi at 3.5 GHz. The four probe antennas are selected from a 16×16 uniform rectangular array with an element spacing of 108 mm, as illustrated in Fig. 7.
- DUT composed of 4 axial quad ridged horn antennas.
- a single pole quad throw switch.
- a master computer to set magnitude and phase values in the control network and to communicate with the VNA.

In this paper, wireless cable connections for a DUT with 4 antennas with $K = 4$ is demonstrated (i.e. with only four probe antennas selected), due to limited measurement time we had in the practical measurement. Note that the proposed algorithm in Section II can be applied for a high-order MIMO configuration in principle. The vertically polarized antenna ports of the probe antennas are connected to the magnitude and phase control network. As shown in Fig. 8, both the probe antenna array and the DUT antenna array are four-cell linear arrays with a spacing of 108 mm. The DUT antennas and probe antennas are aligned and facing each other in the measurement with a short distance of 10 cm. The mutual coupling between antenna elements in each linear array at 3.5 GHz is below -30 dB. The whole measuring system is arranged in an anechoic chamber. A frequency sweep from 3 GHz to 4 GHz with 1601 frequency samples was set in the VNA, with an intermediate frequency (IF) bandwidth of 2 KHz and transmit power of 10 dBm. The digital phase shifters with 8 bits convering 360° phase range and the programmable attenuators with a 1 dB LSB covering a 60 dB dynamic range are used in the mesurement system. Note that phase shifters are not ideal in practice, which will introduce errors for different phase states. An amplitude uncertainty within $[-0.5, 0.5]$ dB and a phase uncertainty within $[-5^o, 5^o]$ might exist for each phase state according to the data sheet.

Note that the probe antennas are intentionally placed in the near-field of the DUT antenna (i.e. 10 cm in the measurement), to demonstrate that the proposed testing method works in a compact anechoic box. This is a major advantage in practical setup, since conventional MPAC setups typically require far-field distance for the measurement range.
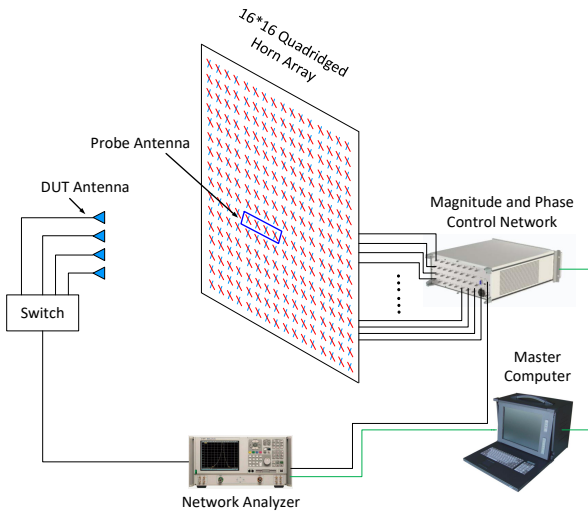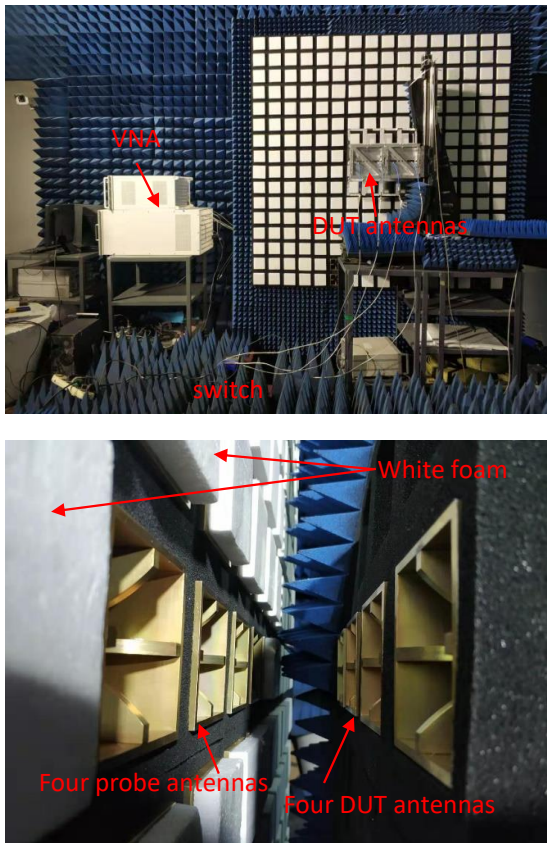
Figure 7. An illustration of the measurement system.

Figure 8. A photo of the measurement system (top) and a photo of the probe antenna and DUT antenna configuration (below).

B. On-off reference measurements

With the measurement system presented in Fig. 7, the coupling coefficients between the four probe antenna ports and the four DUT antenna ports can be directly measured to compose the coupling coefficient matrix $\boldsymbol{A}$. The on-off operation is performed as below. At the probe antenna side, one probe antenna can be enabled via setting 0 dB attenuation in the attenuator associated with the respective probe and all the other probe antennas are disabled via setting 60 dB attenuation in the other attenuators. The phase shifters are set to 0° to all probe antennas in the on-off measurements. The full coupling coefficient matrix $\boldsymbol{A}$ can be recorded in four on-off measurements. The measured 16 coupling coefficients centered at 3.5 GHz with 100 MHz bandwidth in the on-off measurements are shown in Fig. 9. Let us denote the links between the probe antennas and the DUT antennas facing each other as the direct links (e.g. 'OTA 1 - DUT 1', 'OTA 2 - DUT 2', etc.), and the other links between the probe antenna and DUT antennas as undesired cross-talks. An isolation up to 5 dB can be achieved with the measurement setup shown in Fig. 8, due to the directivity of the probe antennas and DUT antennas. Note that in a more general measurement setup, the desired coupling between direct links can be much weaker than the undesired cross-talks, due to the unknown properties of DUT antennas and propagation environments in compact setups. As explained, a direct measurement of the coupling coefficient matrix $\boldsymbol{A}$ (where both amplitude and phase measurements are required) is typically not supported by commercial systems. The directly measured coupling coefficient matrix is utilized here as a reference to validate the proposed calibration method.

C. Calibration Measurement

1) Calibration measurements: In the on-off reference measurements, the amplitude estimates can be directly obtained as discussed above in $K = 4$ measurements. The phase estimates can be estimated following the proposed calibration procedure in Section II-B. To reduce the measurement time, the number of phase states $Q = 3$ was set. For simplicity, $\phi_1 = 0^o$, $\phi_2 = 90^o$ and $\phi_3 = 180^o$ can be typically selected. However, $\phi_1 = 0^o$, $\phi_2 = 132^o$ and $\phi_3 = 252^o$ were set in our measurement campaign to ensure the best condition number of the matrix $\boldsymbol{W}$ in (6). The phase shifter connected to each probe antenna was set to $\{\phi_1, \phi_2, \phi_3\}$, respectively, while other probe antennas were kept 0° in the associated phase shifters. The power at the four DUT antenna ports were recorded for each phase shifter setting. The procedure is repeated for all $K = 4$ OTA antennas, which results in a total of $3K$ measurements. However, the measurements with 0° phase states for all OTA antennas are repeated K times in this procedure. Therefore, $2K + 1$ measurements can be performed with unique phase settings at the phase shifters. Different from the on-off reference measurements (complex field measurements), only power values are recorded per DUT port in the calibration measurements, which is supported by various wireless communication standards.
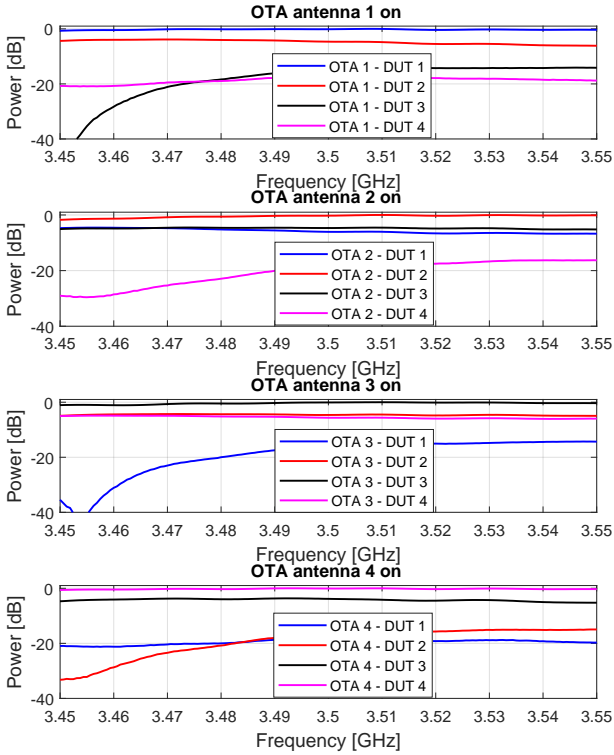
Figure 9. Measured coupling coefficients between the OTA antenna ports and the DUT antenna ports in the on-off reference measurements.

Figure 10. Comparison between measured phase terms of $\boldsymbol{A}$ and $\hat{\boldsymbol{A}}$ at 3.5 GHz.

Figure 11. Measured power levels at DUT antenna ports for the four achieved wireless cable connections with implementing $\hat{\boldsymbol{A}}^{-1}$.

Adopting (8) and (9), the phase estimate $\{\hat{\varphi}_{nk}\}$ can be obtained for $k \in [1, 4]$ and $n \in [1, 4]$. The coupling coefficient matrix $\hat{\boldsymbol{A}}$ is thereby obtained. To evaluate the phase term estimation accuracy, the estimated phase terms of $\hat{\boldsymbol{A}}$ at 3.5 GHz are compared with those of $\boldsymbol{A}$ obtained in the direct on-off reference measurements, as shown in Fig. 10. The phase terms are normolized by the phase term of the first OTA antenna for comparison purpose. This figure shows that the estimated phase terms of $\hat{\boldsymbol{A}}$ agree well with the reference values, where the deviations are within $\pm 9^o$. The deviation is mainly introduced by the non-idealities of the measurement system, e.g. amplitude and phase uncertainties of phase shifters at different phase states.

2) Achieved isolation level: As discussed, the wireless cable connections are realized when the coupling coefficient matrix $\boldsymbol{A}$ is calibrated out via implementing $\hat{\boldsymbol{A}}^{-1}$ in the CE. To investigate to what extent the wireless cable technique works in a practical setup, $\hat{\boldsymbol{A}}^{-1}$ can be implemented with a magnitude and phase control network and validate the achieved isolation levels between DUT antennas. Basically, to achieve the nth wireless cable connection (i.e. signal guided to the nth DUT antenna port with low cross-talks to other DUT antenna ports), K complex weights corresponding to the nth column of $\boldsymbol{A}^{-1}$ to the K probe antennas need to be applied. In the measurement campaign, both $\boldsymbol{A}^{-1}$ and $\hat{\boldsymbol{A}}^{-1}$ were implemented, respectively. The measured power levels at DUT antenna ports for the four achieved wireless cable connections (with $\hat{\boldsymbol{A}}^{-1}$ implemented) are shown in Fig. 11. As seen from the measurement results, the received power levels
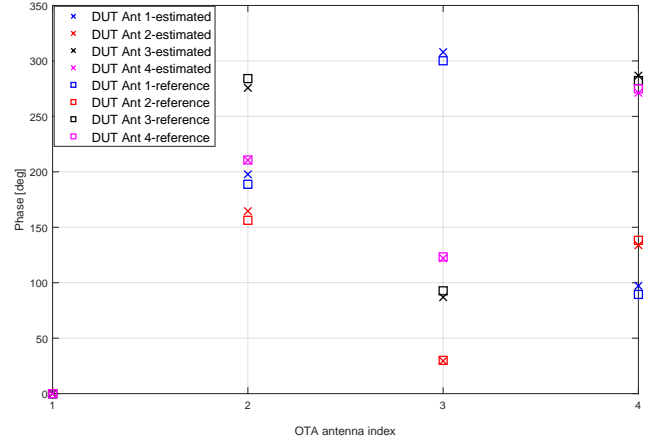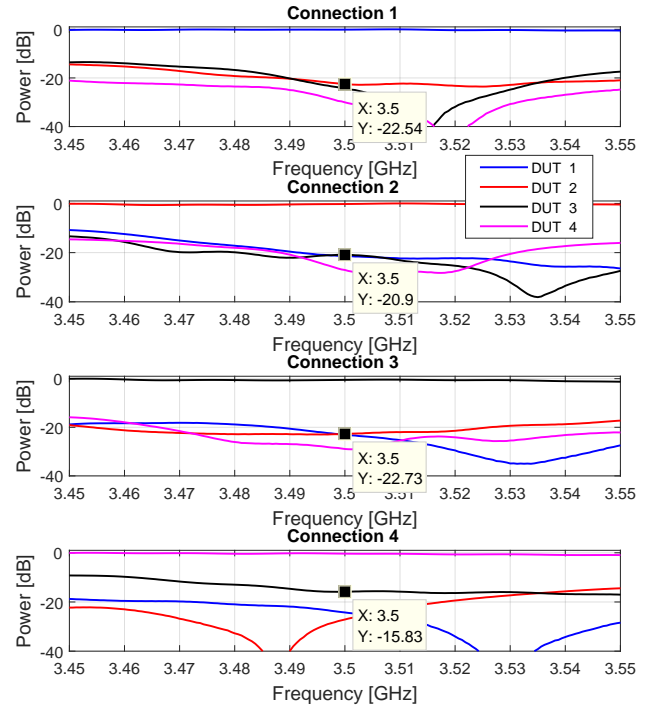
at the direct links are balanced, with -0.1 dB, -0.2 dB,-0.5 dB and -0.4 dB for the direct link 1, 2, 3 and 4, respectively. Isolation levels of 22.4 dB, 20.7 dB, 22.2 dB and 15.4 dB are achieved for the four wireless cable connections, respectively. Compared to the results shown in Fig. 9 where no calibration is performed, the achieved isolation levels are significantly improved. In [21] and [18], it was reported in the throughput measurement results that good wireless cable connections for a 2×2 MIMO system can be achieved when the isolation level is higher than 11 dB and 15 dB, respectively. Therefore, the isolation levels achieved in the measurements are sufficient to achieve wireless cable connections for a 4×4 MIMO system.
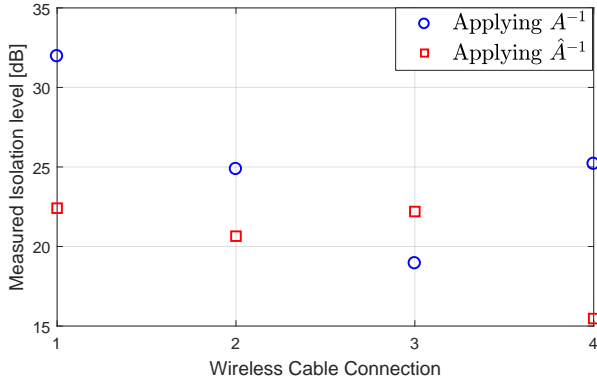
Figure 12. Measured isolation level per wireless cable connection when applying $\boldsymbol{A}^{-1}$ obtained in the on-off reference measurement and $\hat{\boldsymbol{A}}^{-1}$ obtained in the proposed calibration measurement.

The measured isolation levels at 3.5 GHz when applying $\boldsymbol{A}^{-1}$ obtained in the on-off reference measurement and $\hat{\boldsymbol{A}}^{-1}$ obtained in the proposed calibration measurement are compared in Fig. 12. For the reference measurement, an isolation level greater than 19 dB can be achieved for all connections, while an isolation greater than 15.4 dB is obtained for the proposed calibration measurement. Note that even for the reference measurement $|\boldsymbol{A}\boldsymbol{A}^{-1}| = \boldsymbol{I}$ cannot be achieved (corresponding to infinity isolation levels), due to the uncertainty in the phase shifters and the attenuators. As explained in Section II-B, perfectly balanced power between direct links and isolation between direct link and cross-talks can be obtained in principle with the proposed calibration method. However, the results will degrade due to practical implementation of the phase and amplitude control network. Nevertheless, the measurement results demonstrate that a reasonable good power balance and isolation are achieved for the wireless cable connections, despite the uncertainties in phase shifters and attenuators (which leads to the estimation errors in $\hat{\boldsymbol{A}}$ and inaccurately implementing $\hat{\boldsymbol{A}}^{-1}$ in the CE).

V. CONCLUSION

The wireless cable method, which can avoid RF cable connections to the DUT and achieve cable connection functionality, has attracted great research attention. In this paper, a closed-form calibration method is proposed to achieve wireless cable connections for a general $M \times N$ MIMO system equipped with K probe antennas in a shielded measurement setup. With the proposed method, only $3K + 1$ power measurements at the DUT antenna ports (K on-off power measurements for amplitude estimate and $2K+1$ power measurements for phase estimate) are needed with K no less than N, to achieve the wireless cable connections. The theoretical framework is provided, together with experimental validations. The measurement results indicate that the achieved isolation level will be affected by phase shifter and attenuator control accuracy. The proposed method will be highly valuable for MIMO device performance testing. It is highly cost-effective since it only requires a few probe antennas (K) and the measurement setup can be compact. Furthermore, the

solution works for any MIMO devices that support power measurements per DUT antenna port. The MIMO devices can be evaluated under arbitrary propagation channel conditions without extra-cost. At last, the calibration procedure can be carried out within a very short time with the proposed method.

VI. ACKNOWLEDGEMENT

REFERENCES

[1] S.-Y. Lien, S.-L. Shieh, Y. Huang, B. Su, Y.-L. Hsu, and H.-Y. Wei, "5g new radio: Waveform, frame structure, multiple access, and initial access," *IEEE communications magazine*, vol. 55, no. 6, pp. 64–71, 2017.

[2] S. Yi, S. Chun, Y. Lee, S. Park, and S. Jung, *Overview of LTE and LTE-Advanced New Features*. Wiley, 2013. [Online]. Available: https://ieeexplore.ieee.org/document/8043424

[3] K. Technologies, "Testing 5g: Evolution or revolution?" Tech. Rep., October 2016.

[4] X. Chen, "Throughput modeling and measurement in an isotropic-scattering reverberation chamber," *IEEE Transactions on Antennas and Propagation*, vol. 62, no. 4, pp. 2130–2139, April 2014.

[5] X. Chen, J. Tang, T. Li, S. Zhu, Y. Ren, Z. Zhang, and A. Zhang, "Reverberation chambers for over-the-air tests: An overview of two decades of research," *IEEE Access*, vol. 6, pp. 49 129–49 143, 2018.

[6] P. Kyösti, T. Jämsä, and J.-P. Nuutinen, "Channel modelling for multiprobe over-the-air MIMO testing," *International Journal of Antennas and Propagation*, vol. 2012, 2012.

[7] "Test Plan for 2x2 Downlink MIMO and Transmit Diversity Over-the-Air Performance," CTIA Certification, Tech. Rep. Version 1.0, August 2015.

[8] C. Schirmer, M. Lorenz, W. A. T. Kotterman, R. Perthold, M. H. Landmann, and G. D. Galdo, "MIMO over-the-air testing for electrically large objects in non-anechoic environments," in *2016 10th European Conference on Antennas and Propagation (EuCAP)*, April 2016, pp. 1–6.

[9] W. Yu, Y. Qi, K. Liu, Y. Xu, and J. Fan, "Radiated Two-Stage Method for LTE MIMO User Equipment Performance Evaluation," *IEEE Transactions on Electromagnetic Compatibility*, vol. 56, no. 6, pp. 1691–1696, Dec 2014.

[10] Y. Jing, H. Kong, and M. Rumney, "Mimo ota test for a mobile station performance evaluation," *IEEE Instrumentation Measurement Magazine*, vol. 19, no. 3, pp. 43–50, June 2016.

[11] W. Fan, F. Zhang, P. Kyösti, L. Hentilä, and G. F. Pedersen, "Wireless cable method for high-order mimo terminals based on particle swarm optimization algorithm," *IEEE Transactions on Antennas and Propagation*, vol. 66, no. 10, pp. 5536–5545, Oct 2018.

[12] J. Kyrolainen and P. Kyosti, "Systems and methods for calibrating multiple input multiple output (mimo) test systems and for using the calibrated mimo test systems to test mobile devices," Jul. 26 2018, uS Patent App. 15/412,408.

[13] P. Kyosti and J. Kyrolainen, "Systems and methods for radio channel emulation of a multiple input multiple output (mimo) wireless link," Mar. 1 2018, uS Patent App. 15/254,414.

[14] "Further analysis of applicability of RTS to mmWave demodulation testing," Keysight Technologies, Tech. Rep. 3GPP R4-1711501, October 2017.

[15] "Further analysis of RTS applicability to BS demodulation performance testing," Keysight Technologies, Tech. Rep. 3GPP R4-1711501, October 2017.

[16] "Extension of RTS test method from 2Rx to 4Rx and up to 7.25 GHz," Keysight Technologies, Tech. Rep. 3GPP R4-1814834, November 2018.

[17] "RTS system setup for 4x4 MIMO OTA testing," Keysight Technologies, Tech. Rep. 3GPP R4-1900502, March 2019.

[18] W. Fan, P. Kyösti, L. Hentilä, and G. F. Pedersen, "Mimo terminal performance evaluation with a novel wireless cable method," *IEEE Transactions on Antennas and Propagation*, vol. PP, no. 99, pp. 1–1, 2017.

[19] H. Gao, W. Wang, W. Fan, Y. Wu, Y. Liu, and G. F. Pedersen, "Over-the-air testing for carrier aggregation enabled mimo terminals using radiated two-stage method," *Ieee Access*, vol. 6, pp. 71 622–71 631, 2018.

[20] "Verification of radiated multi-antenna reception performance of User Equipment (UE)," 3rd Generation Partnership Project, Tech. Rep. 3GPP TR 37.977 V14.0.0, June 2016.

[21] M. Rumney, Hongwei Kong, Ya Jing, Zheng Zhang, and P. Shen, "Recent advances in the radiated two-stage mimo ota test method and its value for antenna design optimization," in *2016 10th European Conference on Antennas and Propagation (EuCAP)*, April 2016, pp. 1–5.
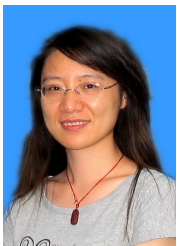
Fengchun Zhang received her B.Sc. degree in optical information science and technology, and the M. Sc. in acoustics from the South China University of Technology, Guangzhou, China, in 2006 and 2009, respectively. She received her Ph.D degree from Aalborg University, Denmark in 2019. She is currently a postdoctoral fellow with the Department of Electronics Systems, Aalborg University, Denmark. Her research interests are in antenna array signal processing, beamforming, parameter estimation for channel characterization of centimeter and millimeter wave wireless systems, and over the air testing.
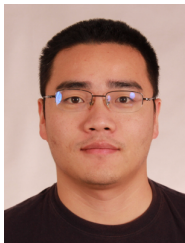
Wei Fan received the B.E. degree from the Harbin Institute of Technology, Harbin, China, in 2009, the master's double degree (Hons.) from the Politecnico di Torino, Turin, Italy, and the Grenoble Institute of Technology, Grenoble, France, in 2011, and the Ph.D. degree from Aalborg University, Aalborg, Denmark, in 2014. In 2011, he joined Intel Mobile Communications, Aalborg, Denmark, as a Research Intern. He conducted a three-month internship at Keysight Technologies, Oulu, in 2014. He is currently an Associate Professor with Aalborg University, Denmark. His current research interests include over-the-air (OTA) testing of multiple antenna systems, radio channel sounding, parameter estimation, modeling, and emulation.
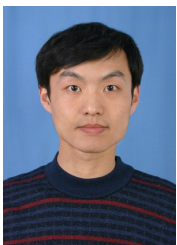
Zhengpeng Wang was born in Shandong, China, in 1981. He received the B.Sc. degree in electronic science and technology from Shandong University, Jinan, China, in 2004, and the M.Sc. and Ph.D. degrees in electromagnetic field and microwave technology from Beihang University, Beijing, China, in 2007 and 2012, respectively. He was a Visiting Researcher with the Antenna and Applied Electromagnetic Laboratory, University of Birmingham, Birmingham, U.K., in 2009 and 2010. From 2013 to 2015, he was a Research Fellow with the University of Kent, Canterbury, U.K., and the University of Science and Technology Beijing, Beijing, China. He is currently an Associate Professor with Beihang University. His current research interests include reconfigurable filters, reconfigurable antennas, filtering antennas, feed antennas, and 5G OTA measurement.